

Pseudo-random sequences for low-cost operando impedance measurements of Li-ion batteries

Jussi Sihvo, Noël Hallemans, Ai Hui Tan, David A. Howey, Stephen. R. Duncan, Tomi Roinila

Abstract—Operando impedance measurements are promising for monitoring batteries in the field. In this work, we present pseudo-random sequences for low-cost operando battery impedance measurements. The quadratic-residue ternary sequence and direct-synthesis ternary sequence exhibit specific properties related to eigenvectors of the discrete Fourier transform matrix that allow computationally efficient compensation for drifts and transients in operando impedance measurements. We describe the application of pseudo-random sequences and provide the data processing required to suppress drift and transients, validated on simulations. Finally, we perform experimental operando impedance measurements on a Li-ion battery cell during fast-charging, demonstrating the applicability of the proposed method. Its low-cost hardware requirements, fast measurements, and simple data-processing make the method practical for embedding in battery management systems.

Index Terms—Lithium-ion battery, Electrochemical impedance spectroscopy, EIS, System identification, Nonlinear distortion, Pseudo-random sequences, BMS

I. INTRODUCTION

LI-ION batteries in electric vehicles and electronic devices require active diagnostics. This is done by battery management systems (BMS) that monitor different states (state-of-health, state-of-charge (SOC), temperature, etc.) to optimise battery management and fast-charging protocols, directly affecting the safety, efficiency, and lifetime of the battery and application. The BMS typically estimates the states from measured current, voltage, and temperature data. Along with these measurements, the impedance is valuable for state monitoring [1]–[3]—mainly due to the separation of time scales corresponding to different physical processes in the battery.

However, impedance data is not widely used in BMS applications. One reason for this is the high implementation cost of conventional electrochemical impedance spectroscopy (EIS) [4], requiring extensive hardware for careful measurements [5], and for generation of sinusoidal excitation. Moreover, conventional EIS measurements can only be performed in

steady-state, which is a general requirement in many system identification applications [6], [7] but rarely occurs in practice for batteries in the field [8]. In the latter situation, impedance must be measured *in operando*—during normal operation of the battery in its host application (e.g. while charging or driving an electric vehicle). However, charging and discharging of the battery can change the local conditions, such as SOC and temperature, which makes the impedance time-varying during experiments [8]. In addition, the battery is never at steady-state, as the charging/discharging current creates voltage drifts, and transient effects are present [9]. All of these have a corrupting effect on the *operando*-measured impedance spectrum, hindering further analysis compared to steady-state conditions.

Existing *operando* EIS methods are based on sinusoidal [10], [11] or multisine (sum-of-sine) [9], [12], [13] excitations. In particular, multisines inject all frequencies simultaneously, which reduces measurement time and minimises the impact of non-stationary conditions compared with conventional EIS [8]. These methods heavily focus on suppressing voltage drifts and modeling time-variation with complex techniques such as the four-dimensional approach [11], wavelet transforms [14], or frequency-domain modelling [9]. Despite the potential and good performance of these methods, the use of multisine (or sine) excitations makes them difficult to apply with low-cost onboard electronics. Moreover, the memory and computational requirements for data processing exceed the majority of BMS processors. Impedance measurement techniques that are technically and economically viable for use in *operando* need to be developed for real-world applications.

An interesting alternative to multisines is provided by pseudo-random sequences (PRS) [15], [16], which have been widely used for identifying electrical motors [17], batteries [18], [19], fuel cells [20], and power-distribution systems [21]. They have several advantages over other excitations: their broadband signal characteristics allow injection of many frequencies simultaneously (minimising measurement time), the sequences typically only have two or three levels (making them relatively easy and cheap to apply in practice), and spectral leakage can be avoided due to periodicity [7]. Moreover, the signal spectrum can be designed to excite a specific set of harmonics, which is useful for identification of nonlinear systems. These properties make PRSs particularly suitable for low-cost impedance measurements for BMS applications.

While reduced hardware costs make PRS methods favorable over multisines for *operando* impedance measurements, the heavy data processing required for drift and transient suppression is still a challenge for BMS applications. However,

This paper has been originally submitted for review on 5th May 2025 to IEEE.

Jussi Sihvo is with the Department of Energy, Aalborg University, Aalborg, Denmark (e-mail: jmesi@energy.aau.dk).

Noël Hallemans, David Howey, and Stephen Duncan are with the Department of Engineering Science, University of Oxford, UK (e-mail: noel.hallemans@eng.ox.ac.uk, david.howey@eng.ox.ac.uk, stephen.duncan@eng.ox.ac.uk).

Ai Hui Tan is with the Faculty of Artificial Intelligence and Engineering, Multimedia University, Cyberjaya, Malaysia (e-mail: htai@mmu.edu.my).

Tomi Roinila is with the Department of Electrical Engineering, Tampere University, Tampere, Finland (e-mail: tomi.roinila@tuni.fi).

some ternary (three-level) pseudo-random sequences exhibit specific properties that enable very simple suppression of voltage drifts and transient effects. These properties are related to the sequences having three levels and being eigenvectors of the discrete Fourier transform (DFT) matrix [22]. Examples of signals with these properties are the quadratic-residue ternary (QRT) sequence [23] and the direct-synthesis ternary (DST) sequence, which has suppressed harmonics for identifying systems exhibiting strong nonlinear distortions [16]. The DST sequence has recently been demonstrated for battery impedance measurements under dynamic current conditions [19]. However, the full theoretical derivation and validation of the DFT eigenvector properties, and drift and transient suppression have not yet been presented.

This paper provides a guide on using QRT and DST sequences for *operando* battery impedance measurements. The theory behind the eigenvector properties is described and illustrative sequences are shown. We explain how these can be implemented in practice and estimate impedance during operation, while suppressing voltage drifts and transients. The proposed method is validated through simulations and experiments from charging of a Li-ion cell. The properties of the presented PRSs enable extraction of impedance during operation within a single excitation period and without complex correction methods. As the methods provide fast measurements with low implementation complexity, they are a pragmatic and economically feasible solution for *operando* impedance measurements in modern high-performance BMS algorithms.

II. TERNARY SEQUENCES WITH DFT EIGENVECTOR PROPERTIES

A. The quadratic-residue ternary (QRT) sequence

The QRT sequence—originating from the Legendre symbol introduced in 1798—is a discrete periodic real-valued ternary sequence of length N_{QRT} defined as [23], [24]

$$u_{\text{QRT}}(n) = \begin{cases} 0 & \text{for } n = 0 \\ 1 & \text{for } n \in \mathbb{S} \\ -1 & \text{else,} \end{cases} \quad (1)$$

with $n = 0, 1, \dots, N_{\text{QRT}} - 1$,

$$\mathbb{S} = \{1^2, 2^2, \dots, (N_{\text{QRT}} - 1)^2\}_{\text{mod } N_{\text{QRT}}}, \quad (2)$$

and N_{QRT} an odd prime satisfying $N_{\text{QRT}} = 4z \pm 1$ with $z \in \mathbb{N}$. We can analyse this sequence in the frequency domain using the normalised DFT given as

$$U_{\text{QRT}}(k) = \frac{1}{\sqrt{N_{\text{QRT}}}} \sum_{n=0}^{N_{\text{QRT}}-1} u_{\text{QRT}}(n) e^{-\frac{j2\pi kn}{N_{\text{QRT}}}}, \quad (3)$$

with $k = 0, 1, \dots, N_{\text{QRT}} - 1$ the harmonic index. Unlike most PRSs, the QRT sequence is an eigenvector of the DFT matrix;

$$\mathbf{U}_{\text{QRT}} = \mathbf{F}\mathbf{u}_{\text{QRT}} = \lambda\mathbf{u}_{\text{QRT}}, \quad (4)$$

with

$$\mathbf{u}_{\text{QRT}} = [u_{\text{QRT}}(0) \ u_{\text{QRT}}(1) \ \dots \ u_{\text{QRT}}(N_{\text{QRT}} - 1)]^{\top}, \quad (5)$$

$$\mathbf{F} = \frac{1}{\sqrt{N_{\text{QRT}}}} \begin{bmatrix} 1 & 1 & 1 & \dots & 1 \\ 1 & w^1 & w^2 & \dots & w^{(N_{\text{QRT}}-1)} \\ 1 & w^2 & w^4 & \dots & w^{2(N_{\text{QRT}}-1)} \\ \vdots & \vdots & \vdots & \ddots & \vdots \\ 1 & w^{N_{\text{QRT}}-1} & w^{2(N_{\text{QRT}}-1)} & \dots & w^{(N_{\text{QRT}}-1)^2} \end{bmatrix}, \quad (6)$$

and $w = e^{-\frac{j2\pi}{N_{\text{QRT}}}}$. For a given vector \mathbf{u}_{QRT} , the associated eigenvalue λ takes *one* out of four (either purely real or purely imaginary) values, depending on the length and symmetry properties of the eigenvector [24],

$$\lambda \in \{1, -1, j, -j\}. \quad (7)$$

This effect is related to the DFT eigenvalue multiplicity problem presented in [22]. The time- and frequency-domain values of the QRT sequence are, hence, correlated,

$$U_{\text{QRT}}(k) = \lambda u_{\text{QRT}}(k) \quad k = 0, 1, \dots, N_{\text{QRT}} - 1. \quad (8)$$

As $u_{\text{QRT}}(n)$ (1) only takes two non-zero values (-1 and 1), it follows from (8) that $U_{\text{QRT}}(k)$ also takes two non-zero values ($-\lambda$ and λ). We now introduce two sets containing the indices at which the non-zero values take place,

$$\begin{aligned} \mathbb{K}_+ &= \{k \mid u_{\text{QRT}}(k) = 1\} \\ \mathbb{K}_- &= \{k \mid u_{\text{QRT}}(k) = -1\}, \end{aligned} \quad (9)$$

and find that

$$U_{\text{QRT}}(k) = \begin{cases} 0 & \text{for } k = 0 \\ \lambda & \text{for } k \in \mathbb{K}_+ \\ -\lambda & \text{for } k \in \mathbb{K}_-. \end{cases} \quad (10)$$

The two non-zero values of $U_{\text{QRT}}(k)$, hence, take place on two sets of intertwined indices, \mathbb{K}_+ and \mathbb{K}_- (9). Moreover, the non-zero values of $U_{\text{QRT}}(k)$ (10) are complements of each other (either λ or $-\lambda$). Hence, from (10) we write that

$$U_{\text{QRT}}(k_+) = -U_{\text{QRT}}(k_-) \quad \forall k_+ \in \mathbb{K}_+ \text{ and } k_- \in \mathbb{K}_-. \quad (11)$$

We will exploit this property for suppressing drift and transient signals in *operando* impedance measurements (Section V).

An example QRT sequence of length $N_{\text{QRT}} = 7$ with eigenvalue $\lambda = -j$ is shown in Fig. 1. The QRT excites all harmonics (except DC) with uniform magnitudes of one, which is common for many types of PRSs used for system identification [25]. The values $U_{\text{QRT}}(k)$ at the harmonics \mathbb{K}_+ (blue, time-domain values of 1) have a phase difference of π compared to the values at harmonics \mathbb{K}_- (red, time-domain values of -1).

B. The direct-synthesis ternary (DST) sequence

The QRT sequence defined above excites all harmonics. However, when identifying nonlinear systems, it is useful to suppress certain harmonics. Suppressing even harmonics allows detection and classification of even and odd nonlinearities and estimation of the best linear approximation of the system [26], [27]. In this section we extend the QRT to suppress second- and third-order harmonics while still satisfying the

III. PRACTICAL MEASUREMENTS WITH PRS SIGNALS

We now detail how to apply the QRT and DST sequences to real-life systems by making them continuous, and how to sample current and voltage data.

Zero-order hold reconstruction

Zero-order hold reconstruction is often used to apply a continuous excitation signal to a system under test [28]. The applied current signal $i(t)$, with t the continuous time, is mathematically obtained by convolving the discrete sequence $u(n)$ with a top-hat function of length T_{zoh} , resulting in the black staircase signals in Figs. 1 and 2, and multiplying with the amplitude of the excitation C ,

$$i(t) = C \text{zoh}_{T_{\text{zoh}}}\{u(n)\}. \quad (22)$$

As a result of the reconstruction, the spectrum of the applied continuous signal $i(t)$ is filtered,

$$I(\omega) = C \text{ZOH}(\omega)U(\omega), \quad (23)$$

with $U(\omega)$ the Fourier transform of the repeated sequence $u(n)$ with intervals T_{zoh} and

$$\text{ZOH}(\omega) = e^{-j\frac{\omega T_{\text{zoh}}}{2}} \text{sinc}\left(\frac{\omega T_{\text{zoh}}}{2}\right). \quad (24)$$

This filtering operation can be visualised in the current spectrum $I(k)$ in Fig. 3. Two important observations should be made:

- The zero-order hold period T_{zoh} sets the bandwidth of the impedance measurement. The period of the excitation is $T_p = N_p T_{\text{zoh}}$, with N_p the length of the QRT or DST sequence. The lowest excited frequency is hence $f_{\text{min}} = 1/T_p$. Regarding the maximal frequency, $I(\omega)$ has a first zero-crossing at $\omega = 2\pi f_{\text{zoh}}$, with $f_{\text{zoh}} = 1/T_{\text{zoh}}$, and has further zero-crossings at all integer multiples. As the magnitude of the excitation already decreases significantly at frequencies lower than f_{zoh} (therefore decreasing the signal-to-noise ratio), we measure impedance up to $f_{\text{max}} = 2f_{\text{zoh}}/3$. In our experiments we set $f_{\text{zoh}} = 1.5$ kHz so that we can measure frequencies up to 1 kHz (as in Fig. 3). For the experiments we use a DST sequence of length $N_p = 10002$, such that $T_p = 10002/1500 = 6.668$ s, and the lowest frequency $f_{\text{min}} = 0.15$ Hz. Note that f_{zoh} here is the same as the “generating frequency”, a commonly used term in many related studies [17]–[21].
- Properties (11) and (20) hold for the discrete sequences, however, they do not hold for the continuous spectrum $I(\omega)$. Instead,

$$I(\omega_{k_+}) = -\frac{\text{ZOH}(\omega_{k_+})}{\text{ZOH}(\omega_{k_-})} I(\omega_{k_-}) \quad \forall \begin{array}{l} k_+ \in \mathbb{K}_+ \\ k_- \in \mathbb{K}_-, \end{array} \quad (25)$$

with $\omega_k = 2\pi k/T_p$. Still, for harmonics k_+ and k_- that are close to each other, we have that $I(\omega_{k_+}) \approx -I(\omega_{k_-})$.

Windowing

To avoid spectral leakage, it is important to measure the applied current and voltage response for an integer number of periods $P \in \mathbb{N}$, that is, within a window $[0, T]$ with $T = PT_p$ and T_p the period of the excitation signal [28]. In this work we use one period ($P = 1$).

Name	Parameter	Value
Sequence length	N_p	10002
Excitation amplitude	C	1 A (2 A for Fig. 4)
Zero-order hold frequency	f_{zoh}	1.5 kHz
Zero-order hold period	T_{zoh}	666.7 μ s
Period length	T_p	6.668 s
Lowest frequency	f_{min}	0.15 Hz
Highest frequency	f_{max}	1 kHz
Sampling frequency	f_s	150 kHz
Sampling period	T_s	6.667 μ s
Number of periods	P	1
Measurement time	T	6.668 s
Number of data points	N	1.0002e6

TABLE I
MEASUREMENT PARAMETERS FOR THE SIMULATIONS AND MEASUREMENTS WITH DST SEQUENCE.

Sampling

The windowed applied current $i(t)$ and voltage response of the battery $v(t)$ are sampled at rate f_s to obtain time series

$$\begin{aligned} \mathbf{i} &= [i(0) \ i(T_s) \ \dots \ i((N-1)T_s)] \\ \mathbf{v} &= [v(0) \ v(T_s) \ \dots \ v((N-1)T_s)], \end{aligned} \quad (26)$$

with sampling period $T_s = 1/f_s$ and number of samples $N = T/T_s = PN_p f_s / f_{\text{zoh}}$.

The sampling frequency f_s is typically chosen larger than twice the maximum frequency in the measured signal to avoid aliasing. However, the QRT and DST sequences are not band-limited, and, hence, aliasing can only be avoided by using an anti-aliasing filter at a frequency $f_N > f_{\text{max}}$ and sampling at $f_s > 2f_N$. If no anti-aliasing filter is available in the measurement setup, aliasing cannot be avoided. However, one can suppress the effect of alias by oversampling. In our measurements, we oversample by a factor 100 ($f_s/f_{\text{zoh}} = 100$) such that aliased spectra are attenuated by at least a factor 100. Note that oversampling also improves the signal-to-noise ratio.

The measurement parameters discussed above that will be used for simulations and measurements with a DST sequence are listed in Table I.

IV. STEADY-STATE IMPEDANCE MEASUREMENTS

Batteries are nonlinear time-varying systems [8]. However, when in steady-state and driven by a sufficiently small zero-mean excitation, they will approximately behave as linear time-invariant systems. We exploit this to measure impedance with ternary sequences.

Let the excitation current signal $i_{\text{exc}}(t)$ be a periodic ternary sequence (reconstructed with a zero-order hold) with period T_p and sufficiently small amplitude C . The voltage response of the linear time-invariant system is [8]

$$v(t) = \text{OCV} + \mathcal{F}^{-1}\{Z(\omega)I_{\text{exc}}(\omega)\}, \quad (27)$$

with OCV the open circuit voltage of the battery, $\mathcal{F}^{-1}\{\cdot\}$ the inverse Fourier transform, $Z(\omega)$ the impedance, and $I_{\text{exc}}(\omega)$ the Fourier transform of $i_{\text{exc}}(t)$.

Measuring input and output signals (26) as detailed in Section III results in data as in Fig. 3, with DFT

$$V(k) = Z(\omega_k)I_{\text{exc}}(k) + L(\omega_k) \quad k > 0, \quad (28)$$

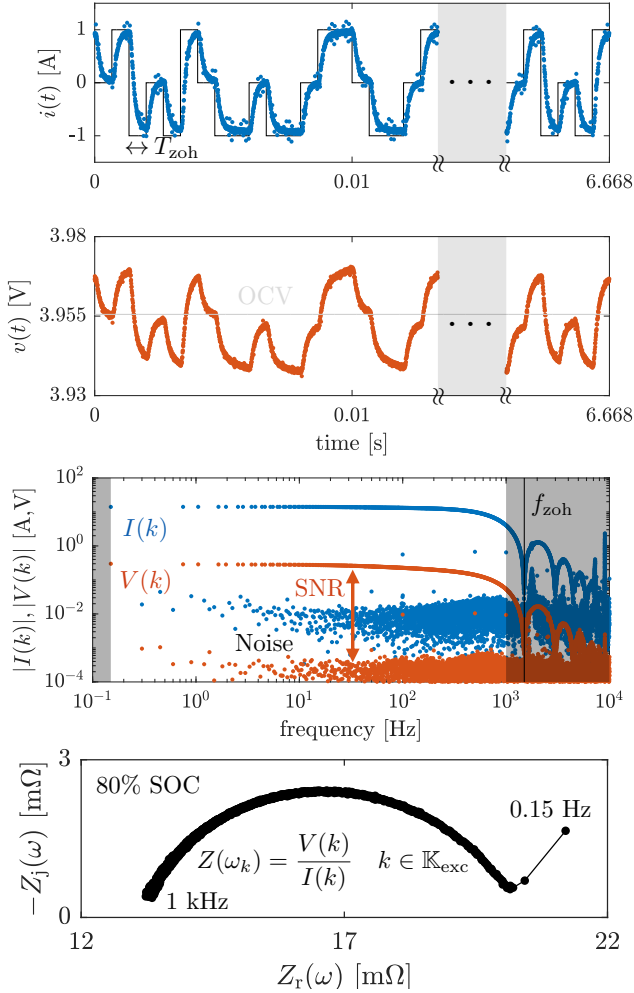


Fig. 3. Measured current, voltage, and impedance data during one steady-state period (after discarding preceding period). From top to bottom: time-domain current- (1) and -voltage profiles (2), their DFT magnitudes (3), and the impedance spectrum (4).

where upper case variables refer to the DFT of the corresponding time domain data, $\omega_k = 2\pi k/T$, and $L(\omega_k)$ is a transient term originating from different initial and end conditions of the finite record [28]. This transient term can easily be removed by discarding the first few periods (e.g. measuring $P = 2$ periods and only applying the DFT on the final one). An impedance estimate is then obtained as

$$\hat{Z}(\omega_k) = \frac{V(k)}{I_{\text{exc}}(k)} \quad k \in \mathbb{K}_{\text{exc}} = P\mathbb{K}, \quad (29)$$

with $\mathbb{K} = \mathbb{K}_+ \cup \mathbb{K}_-$ being the excited harmonics and P the number of periods on which the DFT has been applied.

Measurements also contain noise, and, hence, the signal-to-noise ratio (SNR) should be large enough to measure accurate impedance. The SNR could be improved by increasing the amplitude of the excitation C , but this may result in a nonlinear response—as in Fig. 4, where instead of only having noise at non-excited frequencies, there are also nonlinear distortions. Moreover, as the DST does not excite any second- or third-order harmonics, we can measure the level of even nonlinearities

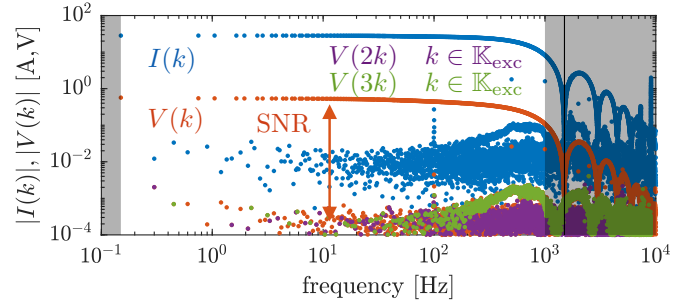


Fig. 4. DFT magnitude spectra of the steady-state current and voltage measurements with highlighted 2nd- and 3rd-order nonlinearities (2 A excitation amplitude).

ties at $V(2k)$ (purple) and odd nonlinearities at $V(3k)$ (green) for $k \in \mathbb{K}_{\text{exc}}$. Odd nonlinearities dominate in this case. An improvement in SNR therefore comes at the cost of increased total harmonic distortion. The best linear approximation can still be obtained by dividing the voltage and current spectra at the excited harmonics (29) [27].

When performing impedance measurements in *operando* conditions, one cannot remove the transient term, and there is often a superimposed drift signal too. The QRT and DST properties (11) and (20) allow suppression of these effects, as discussed in the following section.

V. OPERANDO IMPEDANCE MEASUREMENTS

We now consider the nonlinear time-varying system excited by an input current signal

$$i(t) = i_0(t) + i_{\text{exc}}(t), \quad (30)$$

with $i_0(t)$ being a slowly varying signal to drive the system in normal operating conditions (e.g. constant charging current). Assuming the amplitude C of $i_{\text{exc}}(t)$ is sufficiently small, the system will have a linear *time-varying* response [8],

$$v(t) = v_0(t) + \mathcal{F}^{-1}\{Z(\omega, t)(I_0(\omega) + I_{\text{exc}}(\omega))\}, \quad (31)$$

where $v_0(t)$ is a drift signal [9], $Z(\omega, t)$ is the time-varying impedance, and $I_0(\omega)$ is the Fourier transform of $i_0(t)$. Note that a drift signal and time-varying impedance may also be present when $i_0(t) = 0$, for instance during relaxation or temperature changes.

Consider an experiment over one period of the excitation signal $i_{\text{exc}}(t)$. When the period T_p is sufficiently short, such that the system is approximately time-invariant during the applied period, the output voltage is

$$v(t) = v_0(t) + \mathcal{F}^{-1}\{Z(\omega)(I_0(\omega) + I_{\text{exc}}(\omega))\} \quad t \in [0, T_p], \quad (32)$$

with $Z(\omega)$ being the average of the time-varying impedance during that period,

$$Z(\omega) = \frac{1}{T_p} \int_0^{T_p} Z(\omega, t) dt. \quad (33)$$

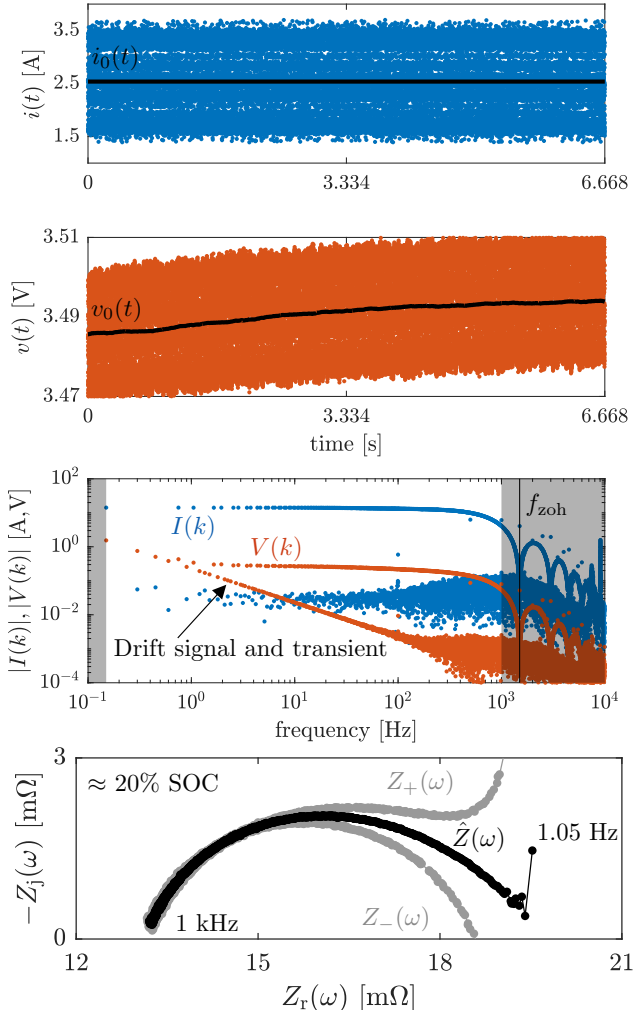


Fig. 5. Measured current, voltage and impedance data during one *operando* period. From top to bottom: time-domain current- (1) and -voltage profiles (2), their DFT magnitude spectra (3), and the impedance spectra (4).

Input-output data over this period was measured with a sampling period T_s resulting in $N_{pp} = T_p/T_s$ data points (see Fig. 5). The DFT of the voltage is

$$V(k) = V_0(k) + Z(\omega_k)(I_0(k) + I_{\text{exc}}(k)) + L(\omega_k), \quad (34)$$

where upper case variables refer to the DFT of the corresponding time domain data and $\omega_k = 2\pi k/T_p$. The transient $L(\omega_k)$ is unavoidable here due to the system not being in steady-state [28], and due to this transient and drift signal $V_0(k)$, we do not obtain an exact measurement of the impedance $Z(\omega_k)$ by dividing $V(k)$ and $I_0(k) + I_{\text{exc}}(k)$ at the excited harmonics \mathbb{K} (29). We now study removal of the effects of drifts and transients.

A. Repeated experiments for drift and transient removal

Consider two experiments carried out under exactly the same (initial) conditions, but with two different input signals,

$$\begin{aligned} i_+(t) &= i_0(t) + i_{\text{exc}}(t) \\ i_-(t) &= i_0(t) - i_{\text{exc}}(t), \end{aligned} \quad (35)$$

sampled for one period and with DFTs $I_{\pm}(k)$. The voltage response of these two experiments $v_{\pm}(t)$ is sampled for one period, and yields DFTs $V_{\pm}(k)$. At the excited harmonics \mathbb{K} one can measure

$$\begin{aligned} Z_{\pm}(\omega_k) &= \frac{V_{\pm}(k)}{I_{\pm}(k)} \quad k \in \mathbb{K} \\ &= \frac{V_0(k) + Z(\omega_k)(I_0(k) \pm I_{\text{exc}}(k)) + L(\omega_k)}{I_0(k) \pm I_{\text{exc}}(k)}. \end{aligned} \quad (36)$$

Note that the same transient term $L(\omega_k)$ is used for the two different excitations. The sign change of $i_{\text{exc}}(t)$, however, may lead to a (small) difference in end conditions, and, hence, a slightly different transient term. We assume that the effect of the initial conditions in the transient is dominant, and that the effect of the sign of $i_{\text{exc}}(t)$ on the end conditions is negligible. Rearranging these equations, the impedance $Z(\omega_k)$ can be retrieved from $Z_+(\omega_k)$, $Z_-(\omega_k)$, $I_0(k)$, and $I_{\text{exc}}(k)$:

$$Z(\omega_k) = \frac{Z_+(\omega_k) + Z_-(\omega_k)}{2} + \frac{I_0(k)}{2I_{\text{exc}}(k)}(Z_+(\omega_k) - Z_-(\omega_k)). \quad (37)$$

Moreover, when $i_0(t)$ is a constant ($I_0(k) = 0$ for $k > 0$), (37) is reduced to

$$Z(\omega_k) = \frac{Z_+(\omega_k) + Z_-(\omega_k)}{2} \quad k \in \mathbb{K}. \quad (38)$$

This means that one can suppress the effects of the drifts and transients when performing two separate experiments with opposite sign of $i_{\text{exc}}(t)$, under identical (initial) conditions. This may, however, be difficult in practice. Instead, the QRT and DST sequences can be used to suppress drifts and transients from a single experiment, which is discussed next.

B. Use of the QRT and DST sequences

Property (20) of the DST (and QRT) sequence allows use of (37) to suppress the drift and transient effects in a single experiment. Let an excitation $i(t) = i_0(t) + i_{\text{exc}}(t)$ be applied to the system with $i_{\text{exc}}(t)$ being a scaled QRT or DST sequence. For $k_+ \in \mathbb{K}_+$ and $k_- \in \mathbb{K}_-$ being close to each other, the effect of the zero-order hold in (25) is negligible and the DFT of the excitation satisfies

$$I_{\text{exc}}(k_+) \approx -I_{\text{exc}}(k_-). \quad (39)$$

Alternatively, the zero-order hold effects can be taken into account for increased accuracy. Next, let the measured current and voltage data have DFTs $I(k)$ and $V(k)$, respectively. An estimate of the impedance, with drifts and transients suppressed, can be obtained as

$$\hat{Z}(\omega_k) = \frac{Z_+(\omega_k) + Z_-(\omega_k)}{2} + \frac{I_0(k)}{2\tilde{I}(k)}(Z_+(\omega_k) - Z_-(\omega_k)) \quad (40)$$

for $k \in \mathbb{K}$ and with

$$\begin{aligned} Z_+(\omega_k) &= \begin{cases} \frac{V(k)}{I(k)} & \text{for } k \in \mathbb{K}_+ \\ \text{interpolated} & \text{for } k \in \mathbb{K}_- \end{cases} \\ Z_-(\omega_k) &= \begin{cases} \text{interpolated} & \text{for } k \in \mathbb{K}_+ \\ \frac{V(k)}{I(k)} & \text{for } k \in \mathbb{K}_- \end{cases} \\ \tilde{I}(k) &= \begin{cases} I_{\text{exc}}(k) & \text{for } k \in \mathbb{K}_+ \\ \text{interpolated} & \text{for } k \in \mathbb{K}_-. \end{cases} \end{aligned} \quad (41)$$

This is similar to (37), however, instead of doing two experiments we take the values $Z_+(\omega_k)$ from the frequency indices \mathbb{K}_+ and values $Z_-(\omega_k)$ from the indices \mathbb{K}_- (as the excitation contains a sign change between these indices (20)). Because we do not have data for $Z_{\pm}(\omega_k)$ at the harmonics \mathbb{K}_{\mp} (measurements can only be taken at harmonics \mathbb{K}_{\pm}), gaps are filled using interpolation, e.g. linear interpolation. Fig. 5 illustrates this via the components $Z_{\pm}(\omega_k)$ (grey) and the reconstructed impedance $Z(\omega_k)$ (black). The simple division of spectra would have caused the impedance to jump between the two grey components, but using the technique detailed above enables suppression of transients and drift (mainly present at low frequencies).

Discussion of the proposed method

Consider what assumptions for the interpolation in (41) are reasonable. From (36),

$$Z_{\pm}(\omega_k) = Z(\omega_k) + \frac{V_0(k) + L(\omega_k)}{I_0(k) + I_{\text{exc}}(k)} \quad \text{for } k \in \mathbb{K}_{\pm}. \quad (42)$$

Interpolation is reasonable when the impedance $Z(\omega)$, the drift signal $V_0(k)$, the transient $L(\omega)$, slow excitation $I_0(k)$, and $I_{\text{exc}}(k)$ are smooth over the excited frequencies, and the distance between non-zero harmonics is sufficiently small. The input spectrum $I_{\text{exc}}(k)$ is smooth over the excited harmonics \mathbb{K}_{\pm} as long as zero crossings are avoided in (23), which is the case as we only consider frequencies up to $2f_{\text{zoh}}/3$ while the first zero-crossing is at f_{zoh} . When the impedance is smooth, the transient is also smooth [7]. The arbitrary excitation $I_0(k)$ is chosen by the user, and the drift signal depends on the system. For battery experiments, the interpolation error will typically be worst at low frequencies.

The interpolation of $Z_+(\omega_k)$ at $k \in \mathbb{K}_-$ and $Z_-(\omega_k)$ at $k \in \mathbb{K}_+$ cannot be applied for indices

$$k < \max(\min(\mathbb{K}_+), \min(\mathbb{K}_-)) \quad (43)$$

$$k > \min(\max(\mathbb{K}_+), \max(\mathbb{K}_-)). \quad (44)$$

Indeed, for these harmonics we would have to *extrapolate* instead of *interpolate*, which can be difficult. The high-frequency bound (44) is not an issue as these harmonics should anyhow be omitted from the results as these harmonics are close to f_{zoh} and, thus, have no energy. However, at the low frequencies (43), one typically loses one or two harmonics depending on the applied sequence.

In the results shown in Fig. 5, the slow signal $i_0(t)$ was a constant charging current of 2.5 A. However, it can be any type of non-periodic signal and typically dictated by the

application. Since the perturbation $i_{\text{exc}}(t)$ is user-defined, it can be subtracted from the measured data $i(t)$ to obtain an estimate for $i_0(t)$ and hence also $I_0(k)$ which, by default, may be unknown.

Several signals including PRSs or multisines are suitable excitations $i_{\text{exc}}(t)$ for steady-state experiments. However, *in operando*, more advanced frequency-domain modelling techniques are usually required to suppress drifts and transients [9], [29]. The use of QRT or DST sequences allows suppression of these drifts and transients with a single experiment and lightweight computations (40), making them feasible for practical use (e.g., BMS applications).

VI. VALIDATION IN SIMULATION

We now validate the impedance reconstruction method via simulation. The model considered is an impedance superimposed on the SOC-dependent OCV, as in (32). The impedance is a simple equivalent circuit model illustrated in Fig. 6 with series resistance R_0 and two RC -branches representing the charge transfer dynamics of the two electrodes. Accordingly, the impedance is

$$Z(\omega) = \frac{b_2(j\omega)^2 + b_1j\omega + b_0}{a_2(j\omega)^2 + a_1j\omega + 1} \quad (45)$$

with

$$\begin{aligned} b_2 &= R_s R_1 R_2 C_1 C_2 \\ b_1 &= R_1 C_1 (R_2 + R_0) + R_2 C_2 (R_1 + R_0) \\ b_0 &= R_1 + R_2 + R_0 \\ a_2 &= R_1 R_2 C_1 C_2 \\ a_1 &= R_1 C_1 + R_2 C_2, \end{aligned} \quad (46)$$

and component values $R_0 = 5 \text{ m}\Omega$, $R_1 = 8 \text{ m}\Omega$, $C_1 = 0.1 \text{ F}$, $R_2 = 20 \text{ m}\Omega$, and $C_2 = 1 \text{ F}$. The drift signal is obtained from OCV data

$$v_0(t) = \text{OCV}(\text{SOC}(t)) \quad (47)$$

where

$$\text{SOC}(t) = \text{SOC}_0 + \frac{100}{3600Q} \int_0^t i(\tau) d\tau, \quad (48)$$

with $Q = 5 \text{ Ah}$ being the battery capacity. As a slow charging current we choose

$$i_0(t) = 2.5 - \frac{t}{2T_p}. \quad (49)$$

We assume the measurement parameters of Table I, and add zero-mean white Gaussian noise to the measured voltage and current with, respectively, standard deviations of $\sigma_v = 0.5 \text{ mV}$ and $\sigma_i = 0.5 \text{ mA}$. The current and voltage spectra are shown in Fig. 6; drift signals are present in both. The true impedance $Z(\omega)$ is shown in yellow, the components $Z_{\pm}(\omega)$ in grey, and the reconstructed impedance $\hat{Z}(\omega)$ in black. The reconstructed impedance coincides with the true impedance (also notable from the error plot), which validates the proposed method. Because of (43), we lose the first two excited harmonics in the reconstruction, giving a lowest frequency of 1.05 Hz instead of 0.15 Hz.

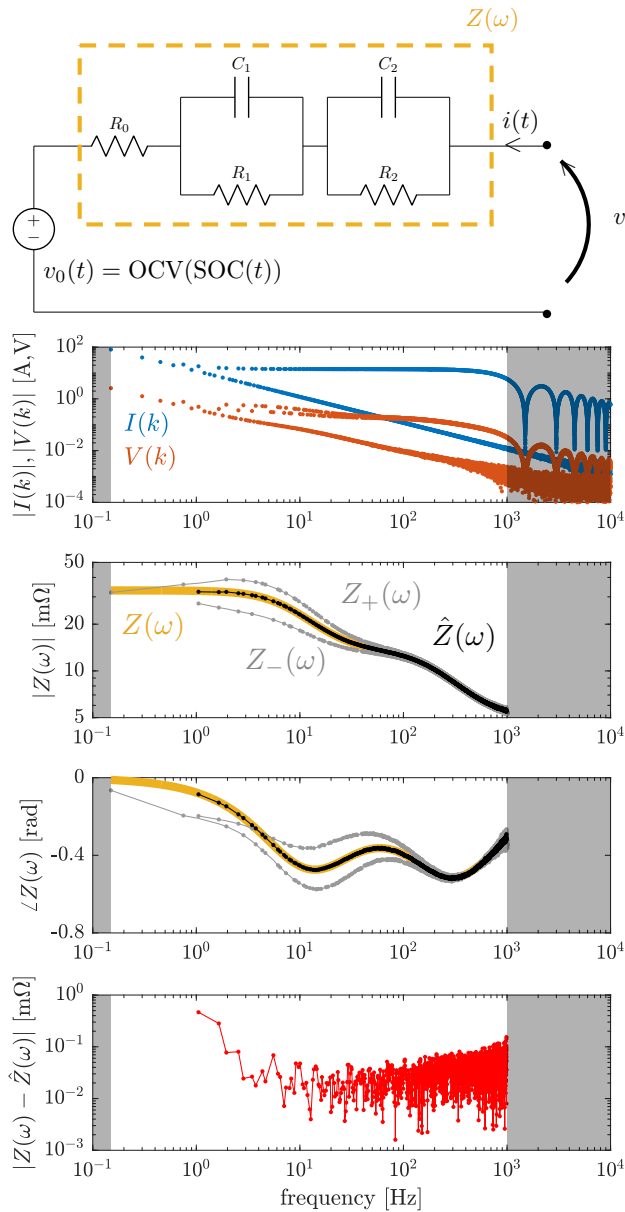


Fig. 6. Results and configuration of the simulations. From top to bottom: Simulation model (1), DFT magnitude spectra of the voltage and current (2), DFT magnitude- (3) and phase spectra (4) of the impedances, and absolute error of the estimated impedance (5).

VII. OPERANDO IMPEDANCE MEASUREMENTS DURING FAST-CHARGING

We now apply the proposed techniques to measure impedance of a Li-ion battery while fast-charging. The battery is a commercial NMC 18650 cell with 3.7 V nominal voltage, 2.5 Ah capacity, and 0.5C of standard charging current. Initially, the cell is at 80% SOC. The cell is connected to a programmable bi-directional power supply to apply the DST perturbation and the fast-charging current. The current and voltage are recorded with a DAQ device synchronised with the applied DST sequence. This cell and measurement setup are also used for the previous measurements (Figs. 3, 4, and 5). A continuous charging current of 2.5 A (1C) was applied

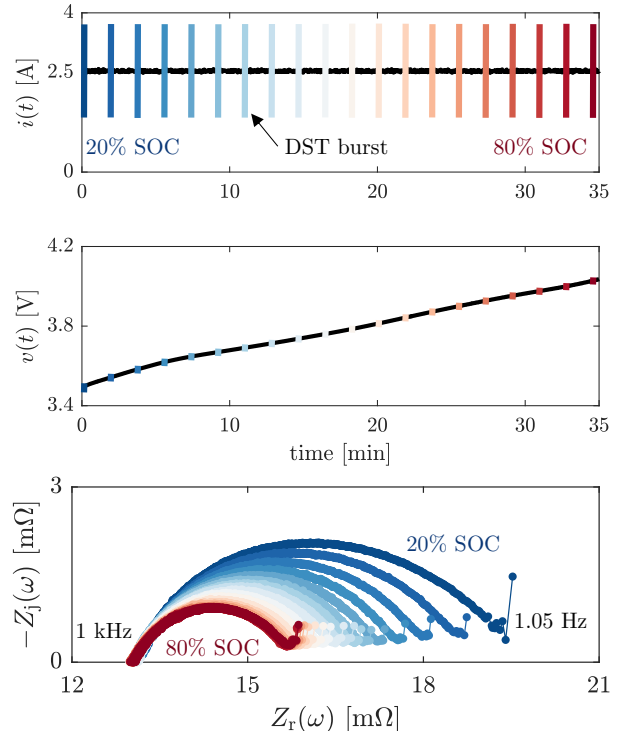


Fig. 7. Results of the operando impedance measurements during fast-charging across 20% to 80% of SOC. Top figure: current profile. Middle figure: voltage profile. Bottom figure: measured impedances.

to the cell from 20 to 80% SOC. The current of 1C is twice the standard charging current of the cell which was considered appropriate to replicate fast-charging conditions. A DST excitation burst with a single period of 6.668 s was superimposed on the charging current every 108 s to measure impedance at 20 different SOC levels (Fig. 7). The DST burst and spectrum for the 20% operating point are shown in Fig. 5. We can see that the width of the semi-circles in the impedances decreases with increasing SOC. This is expected as the impedance depends on SOC, but also on temperature, which is increasing during fast-charging [8]. It is noteworthy that the impedance measured in *operando* provides different information compared to impedance at steady-state [9]. This can be noticed from these experiments, where the 80% SOC *operando* impedance has a smaller semi-circle compared to the 80% SOC steady-state impedance of Fig. 3. Although we have applied a constant charging current the method is also applicable for time-varying currents [19], making it possible to measure impedance at different operating points while fast-charging an electric vehicle. The proposed PRS methods are also applicable during relaxation, and arbitrary application use profiles (e.g. during EV driving [19], or energy trading for a stationary battery).

VIII. CONCLUSIONS

Operando impedance measurements are useful for monitoring batteries in the field. In this work, we presented pseudo-random sequences that can be applied with low-cost electronics, allowing measurement of impedance data in operational

conditions with computationally efficient data processing. We discussed the QRT and DST sequences, which are eigenvectors of the DFT matrix at the excited harmonics. This property makes the drifts- and transients-affected impedance spectrum to separate into two components from which the underlying, true impedance can easily be extracted.

This technique is promising for economically feasible impedance measurements within a BMS during fast-charging, relaxation, or even driving. Short bursts of the proposed DST sequence can be applied over a charging current to extract *operando* impedance, with applications ranging from state-of-health prognostics to parametrizing models for fast-charging.

APPENDIX: PROOF OF (16)

Recall the following property of a repeated signal. Let $u(n)$ be a discrete signal with length N and DFT $U(k)$. Assume $u(n)$ is repeated P times, resulting in $u_P(n)$. The DFT of $u_P(n)$ is

$$U_P(k) = \begin{cases} \sqrt{P}U\left(\frac{k}{P}\right) & \text{for } k = 0, P, 2P, \dots, (N-1)P \\ 0 & \text{else.} \end{cases} \quad (50)$$

The vector \mathbf{a} is constructed by repeating the special sequence $\mathbf{u}_{\text{special}} = [0 \ -1 \ -1 \ 0 \ 1 \ 1]$ (12) (with DFT $\mathbf{U}_{\text{special}} = [0 \ j\sqrt{2} \ 0 \ 0 \ 0 \ -j\sqrt{2}]$) N_{QRT} times. Using (50), we find that

$$A(k) = \begin{cases} j\sqrt{2N_{\text{QRT}}} & \text{for } k = N_{\text{QRT}} \\ -j\sqrt{2N_{\text{QRT}}} & \text{for } k = 5N_{\text{QRT}} \\ 0 & \text{else.} \end{cases} \quad (51)$$

The vector \mathbf{b} is generated by repeating a QRT sequence \mathbf{u}_{QRT} 6 times, hence its DFT is

$$B(k) = \begin{cases} \sqrt{6}U_{\text{QRT}}\left(\frac{k}{6}\right) & \text{for } k = 6, 12, \dots, 6(N_{\text{QRT}} - 1) \\ 0 & \text{else.} \end{cases} \quad (52)$$

Using the fact that the QRT sequence is a completely multiplicative function [30],

$$u_{\text{QRT}}(n) = \frac{u_{\text{QRT}}([dn]_{\text{mod } N_{\text{QRT}}})}{u_{\text{QRT}}(d)} \quad \text{for } 0 \leq d, n < N_{\text{QRT}}, \quad (53)$$

with $u_{\text{QRT}}(6) = r$ ($r \in \{-1, 1\}$ depending on N_{QRT}), we find that for $n = 0, 1, \dots, N_{\text{QRT}} - 1$

$$\begin{aligned} b(6n) &= u_{\text{QRT}}([6n]_{\text{mod } N_{\text{QRT}}}) = ru_{\text{QRT}}(n) \\ &= \frac{r}{\lambda_{\text{QRT}}} U_{\text{QRT}}(n) = \frac{r}{\sqrt{6}\lambda_{\text{QRT}}} B(6n). \end{aligned} \quad (54)$$

Hence,

$$B(k) = \begin{cases} r\sqrt{6}\lambda_{\text{QRT}}b(k) & \text{for } k = 0, 6, 12, \dots, 6(N_{\text{QRT}} - 1), \\ 0 & \text{else.} \end{cases} \quad (55)$$

Therefore \mathbf{b} is an eigenvector of the DFT at its excited harmonics.

The effect of the element-wise multiplication of $a(n)$ and $b(n)$ in the time-domain (15) corresponds to circular convolution of $A(k)$ and $B(k)$ in the frequency-domain,

$$U_{\text{DST}}(k) = \frac{1}{\sqrt{N_{\text{DST}}}} \sum_{m=0}^{N_{\text{DST}}-1} A(m)B([k-m]_{\text{mod } N_{\text{DST}}}). \quad (56)$$

$A(k)$ has only two non-zero values (51), hence, we have that

$$U_{\text{DST}}(k) = \frac{j}{\sqrt{3}} (B([k - N_{\text{QRT}}]_{\text{mod } N_{\text{DST}}}) - B([k - 5N_{\text{QRT}}]_{\text{mod } N_{\text{DST}}})) \quad (57)$$

$B(k)$ (55) is only non-zero for $k \in \{6, 12, \dots, 6(N_{\text{QRT}} - 1)\}$ (52), hence, the term $B([k - \alpha N_{\text{QRT}}]_{\text{mod } N_{\text{DST}}})$ (with $\alpha = 1$ or 5) is only non-zero when

$$k - \alpha N_{\text{QRT}} = 6p \quad \text{for } k \geq \alpha N_{\text{QRT}} \quad (58)$$

$$k - \alpha N_{\text{QRT}} + N_{\text{DST}} = 6p \quad \text{for } k < \alpha N_{\text{QRT}}, \quad (59)$$

with $p = 1, 2, \dots, N_{\text{QRT}} - 1$. Now, for $N_{\text{QRT}} = 7 + 6q$ ($q \in \mathbb{N}$) (13), $B([k - \alpha N_{\text{QRT}}]_{\text{mod } N_{\text{DST}}}) \neq 0$ for $k \in \mathbb{K}_{\alpha}$ with

$$\mathbb{K}_1 = \{1 + 6p \mid p = 0, 1, \dots, N_{\text{QRT}} - 1\} \setminus N_{\text{QRT}} \quad (60)$$

$$\mathbb{K}_5 = \{5 + 6p \mid p = 0, 1, \dots, N_{\text{QRT}} - 1\} \setminus 5N_{\text{QRT}}. \quad (61)$$

The non-zero values of $U_{\text{DST}}(k)$, hence, occur at the harmonics

$$k \in \mathbb{K} = \{1 + 6p, 5 + 6p \mid p = 0, 1, \dots, N_{\text{QRT}} - 1\} \setminus \{N_{\text{QRT}}, 5N_{\text{QRT}}\}. \quad (62)$$

Using the eigenvector property of b (55), and noting that $b([n - \alpha N_{\text{QRT}}]_{\text{mod } N_{\text{DST}}}) = b(n)$ (for both $\alpha = 1$ and 5) due to the periodicity over N_{QRT} samples and the fact that $N_{\text{DST}} = 6N_{\text{QRT}}$, we find that

$$U_{\text{DST}}(k) = \begin{cases} j\sqrt{2r}\lambda_{\text{QRT}}b(k) & \text{for } k \in \mathbb{K}_1 \\ -j\sqrt{2r}\lambda_{\text{QRT}}b(k) & \text{for } k \in \mathbb{K}_5 \\ 0 & \text{else.} \end{cases} \quad (63)$$

Now, as $a(n)$ is periodic over 6 and we know its values, we find that

$$b(n) = \frac{u_{\text{DST}}(n)}{a(n)} = \begin{cases} u_{\text{DST}}(n) & \text{for } n \in \mathbb{K}_1 \\ -u_{\text{DST}}(n) & \text{for } n \in \mathbb{K}_5 \\ 0 & \text{else,} \end{cases} \quad (64)$$

hence,

$$U_{\text{DST}}(k) = \begin{cases} j\sqrt{2r}\lambda_{\text{QRT}}u_{\text{DST}}(k) & \text{for } k \in \mathbb{K} \\ 0 & \text{else.} \end{cases} \quad (65)$$

This is also valid for the other choice $N_{\text{QRT}} = 5 + 6q$ (13).

REFERENCES

- [1] N. Meddings, M. Heinrich, F. Overney, J.-S. Lee, V. Ruiz, E. Napolitano, S. Seitz, G. Hinds, R. Raccichini, M. Gaberšček, and J. Park, "Application of electrochemical impedance spectroscopy to commercial Li-ion cells: A review," *Journal of Power Sources*, vol. 480, p. 228742, 2020.
- [2] P. K. Jones, U. Stimming, and A. A. Lee, "Impedance-based forecasting of lithium-ion battery performance amid uneven usage," *Nature communications*, vol. 13, no. 1, p. 4806, 2022.
- [3] G. L. Plett and M. S. Trimboli, *Battery management systems, Volume III: Physics-Based Methods*. Artech House, 2023.

- [4] S. Wang, J. Zhang, O. Gharbi, V. Vivier, M. Gao, and M. E. Orazem, "Electrochemical impedance spectroscopy," *Nature Reviews Methods Primers*, vol. 1, no. 1, p. 41, 2021.
- [5] D. A. Howey *et al.*, "Online measurement of battery impedance using motor controller excitation," *IEEE Transaction on Vehicular Technology*, vol. 63, no. 6, pp. 2557–2566, 2014.
- [6] L. Ljung, *System Identification: Theory for the User*. Prentice Hall, 1999.
- [7] R. Pintelon and J. Schoukens, *System Identification: A Frequency Domain Approach*. Hoboken, NJ: John Wiley & Sons, Inc., 2012.
- [8] N. Hallemans, D. Howey, A. Battistel, N. F. Saniee, F. Scarpioni, B. Wouters, F. La Mantia, A. Hubin, W. D. Widanage, and J. Lataire, "Electrochemical impedance spectroscopy beyond linearity and stationarity—A critical review," *Electrochimica Acta*, p. 142939, 2023.
- [9] N. Hallemans, W. D. Widanage, X. Zhu, S. Moharana, M. Rashid, A. Hubin, and J. Lataire, "Operando electrochemical impedance spectroscopy and its application to commercial Li-ion batteries," *Journal of Power Sources*, vol. 547, p. 232005, 2022.
- [10] J. Huang, Z. Li, and J. Zhang, "Dynamic electrochemical impedance spectroscopy reconstructed from continuous impedance measurement of single frequency during charging/discharging," *Journal of Power Sources*, vol. 273, pp. 1098–1102, 2015.
- [11] Z. Stoyanov, "Nonstationary impedance spectroscopy," *Electrochimica Acta*, vol. 38, no. 14, pp. 1919–1922, 1993.
- [12] T. Breugelmans, J. Lataire, T. Muselle, E. Tourwé, R. Pintelon, and A. Hubin, "Odd random phase multisine electrochemical impedance spectroscopy to quantify a non-stationary behaviour: Theory and validation by calculating an instantaneous impedance value," *Electrochimica Acta*, vol. 76, pp. 375–382, 2012.
- [13] D. Koster, G. Du, A. Battistel, and F. La Mantia, "Dynamic impedance spectroscopy using dynamic multi-frequency analysis: A theoretical and experimental investigation," *Electrochimica Acta*, vol. 246, pp. 553–563, 2017.
- [14] W. Li, Q.-A. Huang, C. Yang, J. Chen, Z. Tang, F. Zhang, A. Li, L. Zhang, and J. Zhang, "A fast measurement of Warburg-like impedance spectra with Morlet wavelet transform for electrochemical energy devices," *Electrochimica Acta*, vol. 322, p. 134760, 2019.
- [15] K. Godfrey, *Perturbation Signals for System Identification*. Denver, CO: Prentice Hall, 1993.
- [16] A. H. Tan, "Direct synthesis of pseudo-random ternary perturbation signals with harmonic multiples of two and three suppressed," *Automatica*, vol. 49, no. 10, pp. 2975–2981, 2013.
- [17] H. Vermeulen, J. M. Strauss, and V. Shikoana, "Online estimation of synchronous generator parameters using PRBS perturbations," *IEEE Transactions on Power Systems*, vol. 17, no. 3, pp. 694–699, 2002.
- [18] J. Sihvo, T. Roinila, and D.-I. Stroe, "Novel fitting algorithm for parametrization of equivalent circuit model of Li-Ion battery from broadband impedance measurements," *IEEE Transactions on Industrial Electronics*, vol. 68, no. 6, pp. 4916–4926, 2021.
- [19] J. Sihvo and D.-I. Stroe, "Real-time impedance monitoring of Li-ion batteries under dynamic operating conditions: The discrete fourier transform eigenvector approach," *cell Reports Physical Science*, CellPress, Early Access March, 2025.
- [20] S. Mahlangu and P. Barendse, "Fuel cell stack broadband excitation for online condition monitoring using different switch-mode DC-DC topologies," in *2022 IEEE Energy Conversion Congress and Exposition (ECCE)*, 2022, pp. 1–8.
- [21] T. Roinila, H. Abdollahi, and E. Santi, "Frequency-domain identification based on pseudorandom sequences in analysis and control of DC power distribution systems: A review," *IEEE Transactions on Power Electronics*, vol. 36, no. 4, pp. 3744–3756, 2021.
- [22] J. McClellan and T. Parks, "Eigenvalue and eigenvector decomposition of the discrete Fourier transform," *IEEE Transactions on Audio and Electroacoustics*, vol. 20, no. 1, pp. 66–74, 1972.
- [23] K. Godfrey, H. Barker, and A. Tucker, "Comparison of perturbation signals for linear system identification in the frequency domain," in *IEE Proceedings—Control Theory and Applications*, 1999, pp. 535–548.
- [24] M. Narasimha, K. Sheno, and A. Peterson, "Quadratic residues: Application to chirp filters and discrete fourier transforms," in *ICASSP '76. IEEE International Conference on Acoustics, Speech, and Signal Processing*, vol. 1, 1976, pp. 376–378.
- [25] A. H. Tan and K. R. Godfrey, "The generation of binary and near-binary pseudorandom signals: An overview," *IEEE Transactions on Instrumentation and Measurement*, vol. 51, no. 4, pp. 583–588, 2002.
- [26] J. Schoukens, R. Pintelon, T. Dobrowiecki, and Y. Rolain, "Identification of linear systems with nonlinear distortions," *Automatica*, vol. 41, no. 3, pp. 491–504, 2005.
- [27] J. Schoukens, M. Vaes, and R. Pintelon, "Linear system identification in a nonlinear setting: Nonparametric analysis of the nonlinear distortions and their impact on the best linear approximation," *IEEE Control Systems Magazine*, vol. 36, no. 3, pp. 38–69, 2016.
- [28] J. Schoukens, K. Godfrey, and M. Schoukens, "Nonparametric data-driven modeling of linear systems: Estimating the frequency response and impulse response function," *IEEE Control Systems Magazine*, vol. 38, no. 4, pp. 49–88, 2018.
- [29] R. Pintelon, D. Peumans, G. Vandersteen, and J. Lataire, "Frequency response function measurements via local rational modeling, revisited," *IEEE Transactions on Instrumentation and Measurement*, vol. 70, pp. 1–16, 2020.
- [30] S.-C. Pei, C.-C. Wen, and J.-J. Ding, "Closed-form orthogonal DFT eigenvectors generated by complete generalized Legendre sequence," *IEEE Transactions on Circuits and Systems I: Regular Papers*, vol. 55, no. 11, pp. 3469–3479, 2008.